JACS
JOURNAL OF THE AMERICAN CHEMICAL SOCIETY
Article
pubs.acs.org/JACS

Two-Dimensional Mesoporous Carbon Nanosheets and Their Derived Graphene Nanosheets: Synthesis and Efficient Lithium Ion Storage

Yin Fang,[†] Yingying Lv,[†] Renchao Che,[†] Haoyu Wu,[†] Xuehua Zhang,[‡] Dong Gu,[†] Gengfeng Zheng,[†] and Dongyuan Zhao*[,†]

[†]Laboratory of Advanced Materials, Department of Chemistry and Shanghai Key Laboratory of Molecular Catalysis and Innovative Materials, Fudan University, Shanghai 200433, P. R. China

[‡]Department of Chemical and Biomolecular Engineering, University of Melbourne, Australia

Supporting Information

ABSTRACT: We report a new solution deposition method to synthesize an unprecedented type of two-dimensional ordered mesoporous carbon nanosheets via a controlled low-concentration monomicelle close-packing assembly approach. These obtained carbon nanosheets possess only one layer of ordered mesopores on the surface of a substrate, typically the inner walls of anodic aluminum oxide pore channels, and can be further converted into mesoporous graphene nanosheets by carbonization. The atomically flat graphene layers with mesopores provide high surface area for lithium ion adsorption and intercalation, while the ordered mesopores perpendicular to the graphene layer enable efficient ion transport as well as volume expansion flexibility, thus representing a unique orthogonal architecture for excellent lithium ion storage capacity and cycling performance. Lithium ion battery anodes made of the mesoporous graphene nanosheets have exhibited an excellent reversible capacity of 1040 mAh/g at 100 mA/g, and they can retain at 833 mAh/g even after numerous cycles at varied current densities. Even at a large current density of 5 A/g, the reversible capacity is retained around 255 mAh/g, larger than for most other porous carbon-based anodes previously reported, suggesting a remarkably promising candidate for energy storage.

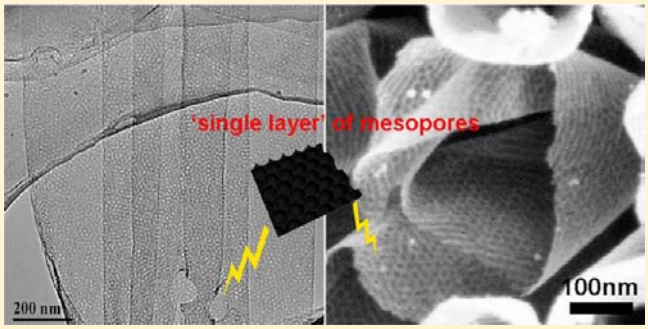

INTRODUCTION

Mesoporous materials represent a large variety of unique structural building blocks with ordered mesochannels, high surface area, and large pore volume, and they exhibit significant potential in many applications, including catalysis, separation, sensing, and energy conversion and storage.[1−9] The synthesis of ordered mesoporous materials can be categorized into two major approaches, known as the soft template and hard template methods, in which mesostructures are preformed by molecular precursors or existing hard templates, followed by structure transformation/replication and template removal. Most of the ordered mesoporous materials investigated, such as hexagonal or cubic structures, are three-dimensional (3D) assemblies with continuous mesostructure frameworks based upon defined space symmetries.[10−16] Nevertheless, pseudo-2D morphologies, such as thin films,[17,18] have intrinsic molecular architectures that are identical to their 3D counterparts. To date, a well-defined 2D mesoporous material with ordered structures and accurate thickness control has not yet been realized.

As an attractive 2D material with remarkable physical and chemical properties,[19−28] graphene has been the focus of substantial research interests. Recently, it has been proposed that the combination of 2D graphene nanosheets with mesoporous architectures can lead to significant enhancement in device performance or new properties.[29−31] For instance, KOH or plasma etching was reported to create porosity in pristine graphene sheets, which were subsequently fabricated as electrical double-layer capacitors[32] or field effect transistors.[33−37] However, the orderings of the obtained mesostructures were generally poor, and the pore sizes were not uniform but in random and wide distribution. In addition, substantial structural defects resulted from these destructive etching methods, limiting the device performance. Therefore, the direct formation of graphene nanosheets with ordered mesostructure, preferably by controlled molecular assembly in a scalable manner, may lead to unconventional material synthesis concepts and device performance enhancement.

In this paper, we demonstrate a novel synthetic approach: low-concentration close-packing assembly[38−41] of monomicelles on a substrate surface to prepare an unprecedented type of 2D ordered mesoporous carbon materials. Monomicelles are first formed as subunits, followed by a hydrothermal treatment

Received: November 4, 2012
Published: January 2, 2013

   dx.doi.org/10.1021/ja310849c | J. Am. Chem. Soc. 2013, 135, 1524−1530

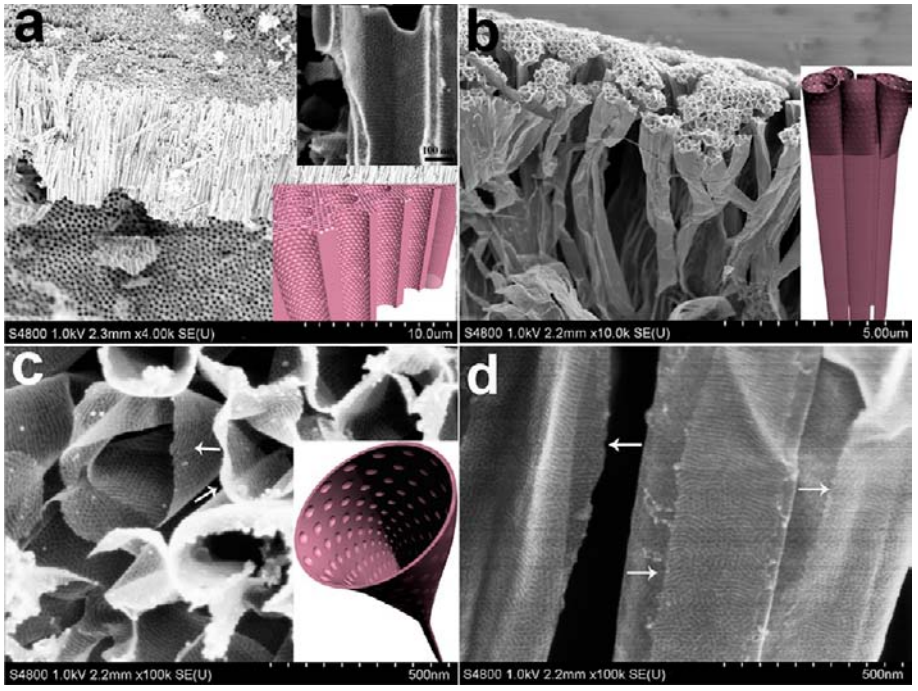

Figure 1. (a) SEM images and schematic (bottom inset) of the mesoporous graphene nanosheets before removal of the AAO template. The remaining regular channels of the membranes are observed. Mesopores grown on the surface of the macroporous channels are ordered on the large domain to form carbon layers several nanometers thick (top inset). (b) SEM images and schematic (inset) of the mesoporous graphene nanosheets after removal of the AAO template. The nanosheet-like morphology grows along the prime AAO channels. (c) SEM images and schematic (inset) of the mesoporous graphene nanosheets observed along the nanosheets. (d) SEM images observed perpendicular to the side walls of the nanosheets. The white arrows indicate that the ultrathin nanosheets are composed of single layers of ordered mesopores.

to assemble these subunits in a close-packing way to form 2D ordered mesoporous carbon nanosheets. Anodic aluminum oxide (AAO) membranes are used as a substrate to provide a large surface area for mass production. In addition, these carbon nanosheets are further converted into mesoporous graphene nanosheets by carbonization at mild temperatures. The obtained 2D mesoporous nanosheets are hundreds of nanometers in width and tens of micrometers in length, corresponding to the internal surface of individual AAO pores, while the sheet thickness is only about 1 nm. The 2D mesoporous nanosheets offer a unique combination of flat graphene layers with large surface area, and abundant ordered mesopores as efficient ion transport pathways, thus allowing for remarkable lithium ion storage capacity and stability. As proof-of-concept, anodes made of the mesoporous graphene nanosheets have shown an ultrahigh initial discharge capacity of 3535 mAh/g at 100 mA/g, stabilized at 770 mAh/g in following cycles. Even at an ultrahigh current density of 5 A/g, a reversible capacity of 255 mAh/g is maintained with excellent cycling stability.

■ EXPERIMENTAL SECTION

Synthesis of Spherical Carbon Monomicelles as Subunits. In a typical synthesis, 0.60 g of phenol, 2.1 mL of formaldehyde solution (37 wt %), and 15 mL of 0.1 M NaOH aqueous solution were mixed and stirred at 70 °C for 0.5 h to obtain low-molecular-weight phenolic resols. After that, 0.96 g of triblock copolymer Pluronic F127 (M_w = 12 600, $PEO_{106}PPO_{70}PEO_{106}$, Acros Corp.) dissolved in 15 mL of H_2O was added and stirred for 2−4 h. Afterward, 50 mL of water was added to dilute the solution and further stirred at 67−70 °C for over 12 h until deposition was observed. During this process, the aqueous solution changed from colorless transparent to pink and finally to crimson. The solution was kept still for further use.

Synthesis of Mesoporous Carbon and Graphene Nanosheets. A hydrothermally driven low-micelle-concentration close-packing method was used to synthesize the ordered mesoporous carbon nanosheets. First, 6.6 mL of the as-prepared monomicelle solution was transferred into an autoclave (50 mL volume), and one piece of the AAO membrane (anodisc 13, 0.2 μm pore size, Whatman Inc.) was put into the solution. The mixture was kept still for 1−3 h for sufficient contact between the AAO membrane and solution. After that, 30 mL of H_2O was added to dilute the solution, and the solution was kept still for 4−6 h. Hydrothermal treatment was then carried out in an oven at 130 °C for 20 h. After cooling down to room temperature, the AAO membrane was taken out from the autoclave, washed with water, and cleaned with wipe paper several times. It was then dried in an oven at 40 °C for 2 days, followed by carbonization at 400−500 °C for 2 h in argon to obtain the mesoporous carbon nanosheets. The mesoporous graphene nanosheets were obtained by further carbonization of the mesoporous carbon nanosheets at 700 °C for 2 h in argon. Finally, the AAO substrates were dissolved and removed by washing with 6 M HCl.

Characterization and Measurements. Transmission electron microscopy (TEM) measurements were conducted on a JEM-2100 F microscope (JEOL, Japan) operated at 200 kV. The mesoporous graphene samples were suspended in ethanol and transferred onto a Cu grid for TEM measurements. Scanning electron microscopy (SEM) images were taken on a Hitachi S-4800 microscope. Atomic force microscopy (AFM) measurements were performed in tapping mode (Multimode IV, Veeco) after the samples were deposited on a freshly cleaved mica surface. A silicon cantilever (TESP-SS, Veeco) with a normal tip radius of <5 nm was used after cleaning in UV/ozone for 15 min. Raman spectra were collected by using Raman microscopes (Renishaw, UK) under 514-nm excitation. Nitrogen sorption isotherms were measured at 77 K with an Autosorb-1MP instrument (Quantachrome, USA). Before measurements, the samples were degassed in a vacuum at 200 °C for at least 12 h.

Electrochemical Evaluation. The electrochemical tests were performed under ambient temperature using two-electrode 2032 coin-

dx.doi.org/10.1021/ja310849c | J. Am. Chem. Soc. 2013, 135, 1524−1530

type cells, and a lithium foil served as the counter electrode. A microporous polypropylene membrane was used as the separator. The working electrode was fabricated by compressing a mixture of the mesoporous graphene nanosheets (active material), acetylene black (conductive agent), and polyvinylidene fluoride (PVDF, binder) in a weight ratio of 85:5:10 onto a copper foil. The electrode was dried at 80 °C for 10 h in a vacuum oven, followed by pressing at 10 MPa. The cell assembly was performed in an argon-filled glovebox in the presence of an oxygen scavenger and a sodium drying agent. The electrolyte solution was 1 M $LiPF_6$ in a mixture of ethylene carbonate (EC), dimethyl carbonate (DMC), and ethyl methyl carbonate (EMC) at a 1:1:1 volume ratio. Electrochemical measurements were taken in a potential range from 3.0 to 0.01 V vs Li/Li^+. Galvanostatic charge/discharge was conducted using a battery tester (Land) at various current rates of 100−5000 mA/g. Cyclic voltammetry (CV) tests were conducted on a CHI760 electrochemistry workstation at a scan rate of 0.1 mV/s. The capacity was based on the amount of the active material, not including the weight of the additives in the electrode.

RESULTS AND DISCUSSION

The 2D mesoporous carbon nanosheets can be assembled on a flat substrate (e.g. copper foil) (Figure S1) or on the substrate surface of arbitrary geometry by using resol-Pluronic composite monomicelles as a subunit. A strong interaction between the monomicelles and substrate is preferred. In this work, AAO membranes are selected as the primary substrates for ease of scaling up and producing enough quantity of samples for characterization and subsequent device fabrication (Figure 1a).[42−44] A thin layer with ordered mesopores can be observed on the inner surface of each individual AAO channel (Figure 1a inset), indicating a successful surface coating. After the AAO is dissolved, the membrane morphology is well retained (Figure S2). The membrane consists of assemblies and arrays of nanosheets tens of micrometers long (Figure 1b). Aligned open macropores of 200−300 nm on the bottom part of the nanosheet assemblies are observed, suggesting that these nanosheets are grown on the inner surface of the pristine AAO pore channels. The morphology of the nanosheets is schematically shown in the inset of Figure 1b. High-resolution SEM images from the open macropores (Figures 1c,d and S3) show that the wall thickness of the nanosheets is within a few nanometers. Ordered mesopore arrays with pore diameters about 9 nm on the surface of the ultrathin nanosheets are clearly observed (highlighted by white arrows in Figure 1c). As these nanosheets are too thin to form mesopores of more than one layer, all the mesopores are laid on one plane, resulting in a 2D mesostructure. On the surface of these individual nanosheets (observed perpendicularly), ordered mesopores with a uniform pore size of ∼9 nm are clearly displayed (Figure 1d), arranged over large domains of several hundred nanometers. In addition, some ultrathin stagger structures can be observed from the shrunken and cracked part of the nanosheets (white arrows in Figure 1d), implying that a dual-layered structure of the nanosheets results from the original conformal coating of the mesoporous graphene nanosheets inside the AAO pores.

The structure and thickness of the mesoporous graphene nanosheets are further characterized by AFM (Figure 2). In some cracked parts where the top layer is peeled off by the AFM tip, the bottom layer can be observed, indicating the dual-layered structure of the sample. In this cracked area, the height difference between single and double layers is measured to be about 1 nm, implying that the top layer (as well as the bottom layer) of the nanosheets consists of ∼3 graphene layers,

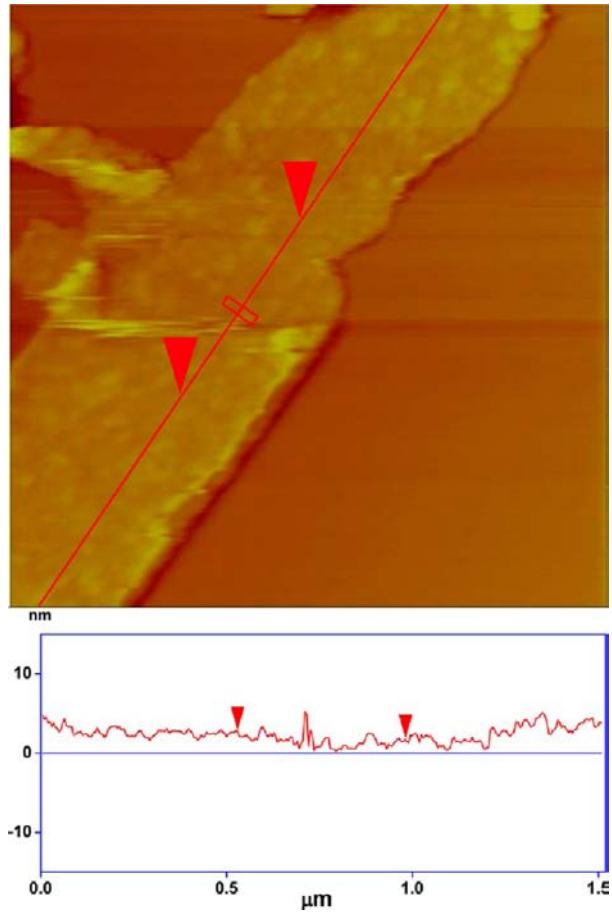

Figure 2. (Top) AFM topography image measured from the cracked area of the mesoporous graphene nanosheets, of which one layer is torn off by the AFM tip. (Bottom) Height difference measured between top and bottom layers is ∼1 nm.

confirming the existence of ultrathin 2D plane-like mesoporous nanosheets.

TEM images show that the carbon nanosheets have an average length of tens of micrometers and a width of 400−500 nm (Figure 3a). The dual-layered structure can be clearly observed in some cracked and staggered portions (red arrows in Figures 3 and S3). These nanosheets clearly display ordered mesostructures, with the average pore size and wall thickness measured to be ∼9 and ∼4 nm, respectively (Figure 3b,c). The bottom part of these mesopores in the nanosheets remains after high-temperature carbonization at 700 °C, resulting in a bowl-like structure (Figure 3c, inset). Meanwhile, no overlay of mesopores is observed in the single-layer nanosheets, suggesting that these mesopores are close-packed on the same plane (Figure S3b,d). However, in some parts of the AAO membranes, such as at the bottom domain of channels and nearby, "lamellar" (linear patterned) mesostructures can also be observed (Figure S3e,f). This phenomenon can be ascribed to the large surface curvatures at these locations, where the monomicelle spheres do not favor the formation of the close-packed mesostructure but pack linearly instead. Therefore, the lamellar mesostructures are constructed and can be retained even after carbonization at 700 °C. After carbonization at 700 °C, these carbon nanosheets are graphitized and converted into mesoporous graphene nanosheets. Due to the ultrathin thickness and ordered mesostructure of the nanosheets, the

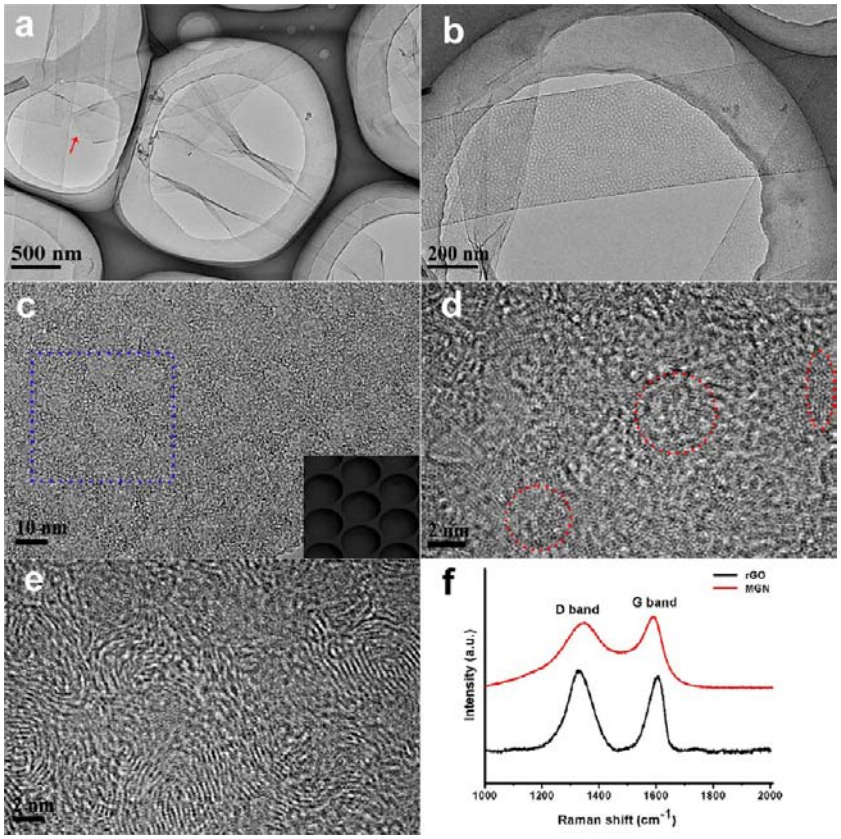

Figure 3. (a–c) TEM and (d,e) HRTEM images of the mesoporous graphene nanosheets synthesized from the low-concentration close-packing assembly of monomicelles. (a) Large-domain observation of the sample. The cracked part is highlighted by the red arrow. (b,c) Mesostructures of the mesoporous graphene nanosheets. The inset in (c) shows the bowl-like mesostructure of the part of the nanosheet highlighted by the blue frame. (d,e) HRTEM images focusing on (d) the bottom plane of the mesopores and (e) the pore walls. Lattices of carbon atoms in different orientations are observed. (f) Raman spectra of the mesoporous graphene nanosheets (red curves) and reduced graphene oxide (black curves). The G band at 1590 cm^{-1} and the D band at 1350 cm^{-1} are labeled in the spectra of the mesoporous graphene nanosheets.

Scheme 1. Schematic of the Formation Process for the Ordered Mesoporous Graphene Nanosheets

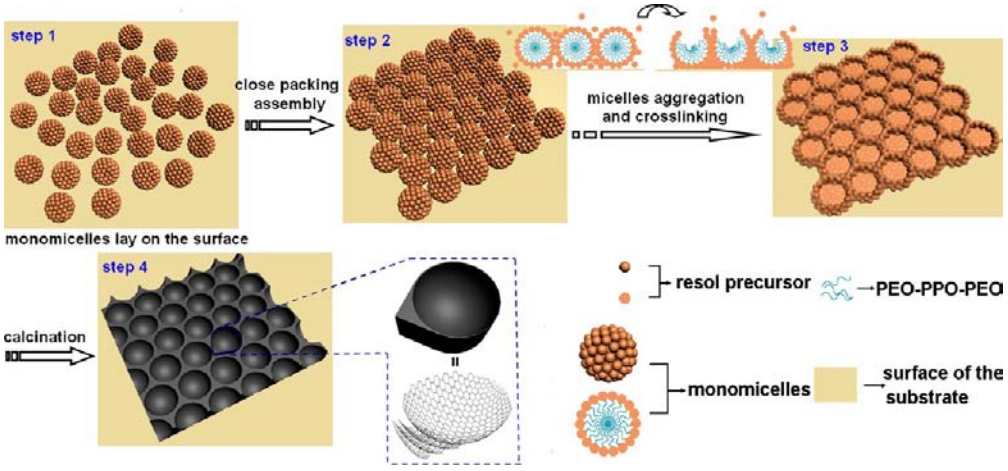

individual carbon atoms can be well resolved in the HRTEM images, arranged in a honeycomb-like structure and some distorted six-member carbon rings (red circles in Figure 3d). These structures have 2–4 repeating units within each nanocrystalline domain. In addition, the lattice-resolved graphite fringes show high crystallinity and substantial curvature; they are aligned around the mesopores and form the pore wall structures (Figure 3e). The spacing between adjacent graphite planes is measured as ~0.336 nm, corresponding to the (002) planes of graphite.

The graphene nature of the obtained mesoporous nanosheets is further confirmed by Raman spectroscopy (Figure 3f). The Raman band at around 1590 cm^{-1} corresponds to the bond stretching of the sp^2 carbon (the G band), and the peak around 1350 cm^{-1} is derived from the breathing mode of aromatic rings (the D band). This result is consistent with typical Raman spectra of graphene oxides and reduced graphene oxides.[45] The

dx.doi.org/10.1021/ja310849c | J. Am. Chem. Soc. 2013, 135, 1524–1530

intense D band shown in the spectra indicates the partial lattice defects of the mesoporous graphene nanosheets compared to single graphene layers, due to the structure distortion to accommodate mesopores. Furthermore, the electron energy loss spectroscopy (EELS) exhibits a characteristic peak at 285 eV and a broadened peak around 293 eV (Figure S4),[32] indicative of the sp^2 and sp^3 carbon bonding contributions in the mesoporous nanosheets, respectively, in good accord with the Raman spectra.

The small-angle X-ray scattering (SAXS) integral curve of the mesoporous graphene nanosheets shows a weak and broad scattering peak around q = 1.2 nm^{-1} (Figure S5a), which may be due to the ultrathin thickness of the nanosheets, as well as stacking between individual nanosheets. The 2D SAXS pattern (Figure S5b) reveals a bright scattering spot in the center with decreased intensity in the circumference, suggesting a heterogeneous nature of the 2D mesoporous nanosheets.

N_2 sorption isotherms show a typical type IV curve with a H2 hysteresis loop, indicating the existence of mesopores. The surface area of the mesoporous graphene nanosheets is calculated to be ~281 m^2/g (Figure S6a), comparable with some reduced graphene oxides prepared by chemical method,[24] but lower than that of the 3D mesoporous carbon materials reported previously.[4] This can probably be ascribed to the stacking of individual mesoporous nanosheets strongly induced by the van der Waals interaction (Figure S6b,c). The pore volume is estimated to be ~0.969 cm^3/g, much larger than that of graphene oxides, which is attributed to the existence of abundant mesopores in these nanosheets.

The formation mechanism of the mesoporous graphene nanosheets is proposed as controlled assembly of monomicelles and heterogeneous nucleation process on the substrate surface (Scheme 1). The as-prepared phenolic resol molecules are first assembled with Pluronic triblock copolymer templates into spherical monomicelles as subunit building blocks and deposited on the surface of substrate (or the channel walls of AAO templates) (step 1) because of the strong interaction between the composite monomicelles and the surface of the substrate. Composed of the low-molecule-weight phenolic resols, the monomicelles are rich in phenolic hydroxyl groups. Thus, in the alkaline solution, these monomicelles are negatively charged and adhered on the substrate surface via the electrostatic attraction. These spherical monomicelles as subunits are continuously deposited, assembled, and then slowly transformed into an ordered micelles array by a close-packing route to form the lowest energy state (step 2). At a low concentration, the tendency of the monomicelle heterogeneous nucleation on the substrate surface via the electrostatic attraction is more favorable than the stacking of monomicelles by spontaneous nucleation, thus a single layer of the monomicelles assembly is formed. Here, the interaction between the resol-Pluronic composite monomicelles and the substrate is a key issue for the single layer assembly, which should be much stronger than that between the monomicelles themselves. The low concentration and strong interaction with the substrates prevent multilayer deposition of the monomicelles from a formation of 3D mesostructure. Under the hydrothermal treatment, these micelles are successively polymerized and aggregated together tightly to form bowl-like structures, which subsequently lead to the 2D plane mesostructure (step 3). Finally, the single-layer mesoporous Bakelite resin polymer is carbonized and graphitized by high-temperature calcination (step 4). The pore wall of the mesoporous carbon is formed from the aggregated part of several monomicelles, resulting in the graphite nanoribbons around the mesopores. In contrast, the bottom surface of the mesopores is derived from single monomicelles, and thus an ultrathin thickness of one to several layers of carbon atoms is obtained.

Due to their graphene frameworks, large surface area, and abundant mesopores for ion diffusion and adsorption, these mesoporous graphene nanosheets can serve as a unique and highly promising substitute for graphite anode in the lithium ion battery (LIB) application. The obtained nanosheets are fabricated as a LIB anode based on a standard fabrication procedure, and their electrochemical storage capacity is evaluated on the basis of the half-cell configuration. At a current density of 100 mA/g, an ultrahigh initial capacity of 3535 mAh/g is recorded, which drops to 1040 mAh/g in the second cycle (Figure 4a). The capacity loss during the first cycle, which has been observed for many mesoporous carbon or graphene-based materials reported previously, is mainly attributed to the decomposition of electrolytes and the formation of a solid−electrolyte interface (SEI) on the surface of electrode materials.[46−50] For our novel mesoporous graphene nanosheets, the ultrathin layer and the porous

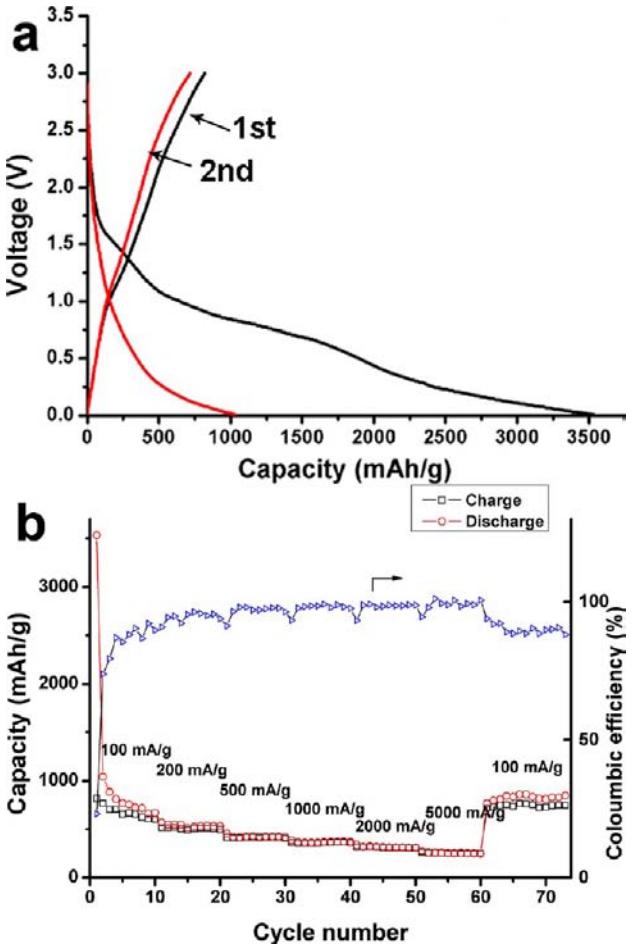

Figure 4. (a) First and second cycles of galvanostatic discharge/charge curves of the mesoporous graphene nanosheets. (b) Cycling performance (red curve, discharge; black curve, charge) and the Coulombic efficiency (blue curve) of the mesoporous graphene nanosheets at different current densities. Each current density is labeled over the corresponding cycles.

dx.doi.org/10.1021/ja310849c | J. Am. Chem. Soc. 2013, 135, 1524−1530

mesostructure greatly increase the efficient contact between the electrolyte and the electrode, thus resulting in enhanced deposition of the SEI layer on the electrode surface. Furthermore, the structural defects introduced during the formation of the mesopores,[44,46,47] together with oxygen-containing functional groups on the surface and residual H atoms[48] produced by the wet etching during the AAO template removal, also contribute to the irreversible capacity, ascribed as a pseudo-capacitive effect. Moreover, the CV plot demonstrates distinct reduction peaks related to the irreversible capacity loss in the first cycle (Figure S7), in good agreement with the first galvanostatic discharge/charge curve. No obvious changes were observed from the second to the fifth cycle of the CV plots, implying good cycling stability.

One major problem for the LIB application is the limited rate performance at high charge/discharge rates. The porous structures have been demonstrated to be beneficial for good rate performance in electrochemical applications.[3,7,32] In addition, it has also been found that the porosity is helpful for improving the rate performance of LIBs.[16,51] For the mesoporous graphene nanosheet samples, owing to the unique ultrathin layer structure with abundant and homogeneous mesopores, lithium ion diffusion can be improved and the diffusion length can be reduced, thus making the products suitable as lithium ion storage materials even at high charge/discharge rates. The cycling performance of the mesoporous graphene nanosheets anode is further evaluated by galvanostatic cycles of different charge/discharge rates. At a current density of 100 mA/g, the reversible capacity of the mesoporous graphene nanosheets is around 770 mAh/g (Figure 4b), almost double the value for graphite (372 mAh/g). The reversible capacity is stabilized at 540, 430, and 370 mAh/g upon increasing the discharge/charge current density to 200, 500, and 1000 mA/g, respectively. At an ultrahigh current density of 5 A/g (13.4C), a large reversible capacity of 255 mAh/g is obtained, with excellent cycling stability. In addition to the high reversible capacities, the Columbic efficiency reaches above 92% after initial 15 cycles. Notably, after 60 cycles at varied current densities, the capacity is retained at 833 mAh/g when the current density is reset to 100 mA/g.

Compared to conventional mesoporous carbon, graphene, and carbon nanotubes,[45−51] the mesoporous graphene nanosheets exhibit not only a substantially larger lithium ion storage capacity but also excellent cycling stability at high current densities. This excellent electrochemical property is attributed to the ultrathin, highly graphitized 2D nanosheet frameworks, as well as the large surface area, and the ordered mesoporous structures. Lithium ions can be electrochemically adsorbed on and intercalated into both sides of the free-standing atomically thin mesoporous carbon nanosheets, as well as the mesopores inside graphene planes, thus providing a higher reversible Li^+ storage capacity than nonporous graphenes. In the orthogonal direction, the open mesopores on the nanosheets offer efficient transport pathways for ion diffusion toward the deep portions of the stacked graphene layers. Moreover, the abundant mesopores further allow for substantial structure and volume flexibility during the Li^+ intercalation, leading to an outstanding storage capacity and stability at a high current density.

CONCLUSION

We have developed a controlled low-concentration monomicelle close-packing assembly approach to synthesize novel ultrathin mesoporous carbon nanosheets. These nanosheets are several micrometers in length, several hundred nanometers in width, and ∼1 nm in thickness. These ultrathin nanosheets are composed of only one layer of ∼9 nm mesopores on the surface of a substrate, typically the inner walls of the AAO pore channels for mass production, and can be directly converted into mesoporous graphene by low-temperature carbonization. It is the first time that a 2D planar mesoporous carbon material has been prepared by using the monomicelles of phenolic resol-Pluronic composites as a subunit. The unique 2D mesoporous structure provides thin graphitic layers for Li ion intercalation, double sides for adsorption, and abundant mesopores as "cavities" to capture extra Li ions, thus leading to remarkable electrochemical properties. Lithium ion battery anodes made of these mesoporous graphene nanosheets have exhibited a high reversible capacity of 770 mAh/g at 100 mA/g. Even at a large current density of 5 A/g (13.4C), the reversible capacity is retained at 255 mAh/g, larger than for most other carbon-based anodes reported previously. Our discovery of 2D mesoporous graphene nanosheets may lead to further development of new device concepts and architectures, thus allowing for more opportunities in realizing novel electrochemical storage with higher power and energy densities.

ASSOCIATED CONTENT

Supporting Information

SEM of ordered 2D mesoporous carbon nanosheets grown on the copper foil; SEM and TEM images from different locations of the mesoporous graphene nanosheets; EELS spectrum, SAXS curves, BET measurement, and CV curves of the mesoporous graphene nanosheets. This material is available free of charge via the Internet at http://pubs.acs.org.

AUTHOR INFORMATION

Corresponding Author

dyzhao@fudan.edu.cn

Notes

The authors declare no competing financial interest.

ACKNOWLEDGMENTS

This work was supported by the State Key Basic Research Program of the PRC (2012CB224805, 2013CB934104), the NSF of China (20890123 and 429 21200004), the Shanghai Leading Academic Discipline Project (B108), the Science and Technology Commission of Shanghai Municipality (08DZ2270500), Delta Company Foundation, and the Scholarship Award for Excellent Doctoral Student granted by Ministry of Education.

REFERENCES

(1) Wan, Y.; Zhao, D. *Chem. Rev.* **2007**, *107*, 2821.
(2) Kresge, C. T.; Leonowicz, M. E.; Roth, W. J.; Vartuli, J. C.; Beck, J. S. *Nature* **1992**, *359*, 710.
(3) Liang, C.; Li, Z.; Dai, S. *Angew. Chem., Int. Ed.* **2008**, *47*, 3696.
(4) Meng, Y.; Gu, D.; Zhang, F.; Shi, Y.; Yang, H.; Li, Z.; Yu, C.; Tu, B.; Zhao, D. *Angew. Chem., Int. Ed.* **2005**, *44*, 7053.
(5) Shi, Y.; Wan, Y.; Zhao, D. *Chem. Soc. Rev.* **2011**, *40*, 3854.
(6) Zhao, D.; Feng, J.; Huo, Q.; Melosh, N.; Fredrickson, G. H.; Chmelka, B. F.; Stucky, G. D. *Science* **1998**, *279*, 548.
(7) Zhai, Y.; Dou, Y.; Zhao, D.; Fulvio, P. F.; Mayes, R. T.; Dai, S. *Adv. Mater.* **2011**, *23*, 4828.
(8) Zheng, Y.; Jiao, Y.; Chen, J.; Liu, J.; Liang, J.; Du, A.; Zhang, W.; Zhu, Z.; Smith, S. C.; Jaroniec, M.; Lu, G. Q.; Qiao, S. Z. *J. Am. Chem. Soc.* **2011**, *133*, 20116.

(9) Liu, R.; Wang, X. Q.; Zhao, X.; Feng, P. Y. *Carbon* **2008**, *46*, 1664.
(10) Lee, J.; Kim, J.; Hyeon, T. *Adv. Mater.* **2006**, *18*, 2073.
(11) Soler-Illia, G. J.; Sanchez, C.; Lebeau, B.; Patarin, J. *Chem. Rev.* **2002**, *102*, 4093.
(12) Fulvio, P. F.; Mayes, R. T.; Wang, X. Q.; Mahurin, S. M.; Bauer, J. C.; Presser, V.; McDonough, J.; Gogotsi, Y.; Dai, S. *Adv. Funct. Mater.* **2011**, *21*, 2208.
(13) Hao, G. P.; Li, W. C.; Qian, D.; Wang, G. H.; Zhang, W. P.; Zhang, T.; Wang, A. Q.; Schuth, F.; Bongard, H. J.; Lu, A. H. *J. Am. Chem. Soc.* **2011**, *133*, 11378.
(14) Lu, A. H.; Hao, G. P.; Sun, Q.; Zhang, X. Q.; Li, W. C. *Macromol. Chem. Phys.* **2012**, *213*, 1107.
(15) Stein, A.; Wang, Z. Y.; Fierke, M. A. *Adv. Mater.* **2009**, *21*, 265.
(16) Vu, A.; Qian, Y. Q.; Stein, A. *Adv. Energy Mater.* **2012**, *2*, 1056.
(17) Innocenzi, P.; Kidchob, T.; Falcaro, P.; Takahashi, M. *Chem. Mater.* **2008**, *20*, 607.
(18) Teng, Z.; Zheng, G.; Dou, Y.; Li, W.; Mou, C. Y.; Zhang, X.; Asiri, A. M.; Zhao, D. *Angew. Chem., Int. Ed.* **2012**, *51*, 2173.
(19) Novoselov, K. S.; Geim, A. K.; Morozov, S. V.; Jiang, D.; Zhang, Y.; Dubonos, S. V.; Grigorieva, I. V.; Firsov, A. A. *Science* **2004**, *306*, 666.
(20) Li, X.; Wang, X.; Zhang, L.; Lee, S.; Dai, H. *Science* **2008**, *319*, 1229.
(21) Yoo, E.; Kim, J.; Hosono, E.; Zhou, H. S.; Kudo, T.; Honma, I. *Nano Lett.* **2008**, *8*, 2277.
(22) Geim, A. K. *Science* **2009**, *324*, 1530.
(23) Kim, K. S.; Zhao, Y.; Jang, H.; Lee, S. Y.; Kim, J. M.; Ahn, J. H.; Kim, P.; Choi, J. Y.; Hong, B. H. *Nature* **2009**, *457*, 706.
(24) Park, S.; Ruoff, R. S. *Nat. Nanotechnol.* **2009**, *4*, 217.
(25) Liao, L.; Lin, Y. C.; Bao, M.; Cheng, R.; Bai, J.; Liu, Y.; Qu, Y.; Wang, K. L.; Huang, Y.; Duan, X. *Nature* **2010**, *467*, 305.
(26) Liu, C.; Yu, Z.; Neff, D.; Zhamu, A.; Jang, B. Z. *Nano Lett.* **2010**, *10*, 4863.
(27) Xiang, Q.; Yu, J.; Jaroniec, M. *Chem. Soc. Rev.* **2012**, *41*, 782.
(28) Liu, Y.; Cheng, R.; Liao, L.; Zhou, H.; Bai, J.; Liu, G.; Liu, L.; Huang, Y.; Duan, X. *Nat. Commun.* **2011**, *2*, 579.
(29) Xiao, J.; Mei, D.; Li, X.; Xu, W.; Wang, D.; Graff, G. L.; Bennett, W. D.; Nie, Z.; Saraf, L. V.; Aksay, I. A.; Liu, J.; Zhang, J. G. *Nano Lett.* **2011**, *11*, 5071.
(30) Liang, J.; Jiao, Y.; Jaroniec, M.; Qiao, S. Z. *Angew. Chem., Int. Ed.* **2012**, *51*, 11496.
(31) Li, X.; Qi, W.; Mei, D.; Sushko, M. L.; Aksay, I.; Liu, J. *Adv. Mater.* **2012**, *24*, 5136.
(32) Zhu, Y.; Murali, S.; Stoller, M. D.; Ganesh, K. J.; Cai, W.; Ferreira, P. J.; Pirkle, A.; Wallace, R. M.; Cychosz, K. A.; Thommes, M.; Su, D.; Stach, E. A.; Ruoff, R. S. *Science* **2011**, *332*, 1537.
(33) Akhavan, O. *ACS Nano* **2010**, *4*, 4174.
(34) Bai, J.; Zhong, X.; Jiang, S.; Huang, Y.; Duan, X. *Nat. Nanotechnol.* **2010**, *5*, 190.
(35) Ning, G.; Fan, Z.; Wang, G.; Gao, J.; Qian, W.; Wei, F. *Chem. Commun.* **2011**, *47*, 5976.
(36) Nguyen, V. H.; Mazzamuto, F.; Saint-Martin, J.; Bournel, A.; Dollfus, P. *Nanotechnology* **2012**, *23*, 065201.
(37) Zeng, Z.; Huang, X.; Yin, Z.; Li, H.; Chen, Y.; Zhang, Q.; Ma, J.; Boey, F.; Zhang, H. *Adv. Mater.* **2012**, *24*, 4138.
(38) Tang, J.; Zhou, X.; Zhao, D.; Lu, G. Q.; Zou, J.; Yu, C. *J. Am. Chem. Soc.* **2007**, *129*, 9044.
(39) Liu, J.; Yang, Q. H.; Zhang, L.; Yang, H. Q.; Gao, J. S.; Li, C. *Chem. Mater.* **2008**, *20*, 4268.
(40) Fang, Y.; Gu, D.; Zou, Y.; Wu, Z.; Li, F.; Che, R.; Deng, Y.; Tu, B.; Zhao, D. *Angew. Chem., Int. Ed.* **2010**, *49*, 7987.
(41) Gu, D.; Bongard, H.; Meng, Y.; Miyasaka, K.; Terasaki, O.; Zhang, F. Q.; Deng, Y. H.; Wu, Z. X.; Feng, D.; Fang, Y.; Tu, B.; Schuth, F.; Zhao, D. Y. *Chem. Mater.* **2010**, *22*, 4828.
(42) Zhi, L.; Wu, J.; Li, J.; Kolb, U.; Mullen, K. *Angew. Chem., Int. Ed.* **2005**, *44*, 2120.
(43) Wu, Y.; Cheng, G.; Katsov, K.; Sides, S. W.; Wang, J.; Tang, J.; Fredrickson, G. H.; Moskovits, M.; Stucky, G. D. *Nat. Mater.* **2004**, *3*, 816.
(44) Wang, K.; Zhang, W.; Phelan, R.; Morris, M. A.; Holmes, J. D. *J. Am. Chem. Soc.* **2007**, *129*, 13388.
(45) Eda, G.; Chhowalla, M. *Adv. Mater.* **2010**, *22*, 2392.
(46) Kaskhedikar, N. A.; Maier, J. *Adv. Mater.* **2009**, *21*, 2664.
(47) Frackowiak, E.; Beguin, F. *Carbon* **2002**, *40*, 1775.
(48) Dahn, J. R.; Zheng, T.; Liu, Y. H.; Xue, J. S. *Science* **1995**, *270*, 590.
(49) Liu, J.; Cao, G.; Yang, Z.; Wang, D.; Dubois, D.; Zhou, X.; Graff, G. L.; Pederson, L. R.; Zhang, J. G. *ChemSusChem* **2008**, *1*, 676.
(50) Guo, B.; Wang, X.; Fulvio, P. F.; Chi, M.; Mahurin, S. M.; Sun, X. G.; Dai, S. *Adv. Mater.* **2011**, *23*, 4661.
(51) Zhao, X.; Hayner, C. M.; Kung, M. C.; Kung, H. H. *ACS Nano* **2011**, *5*, 8739.